TEKNOFEST

AEROSPACE AND TECHNOLOGY FESTIVAL

ENVIRONMENT AND ENERGY TECHNOLOGIES COMPETITION

PROJECT DETAIL REPORT

TEAM NAME: SU-T4E

PROJECT NAME: Novel Anti-icing Coating for Wind Turbines

APPLICATION ID: 434491

Contents

Contents **2**
1. Project summary **3**
2. Problem/ Issue **3**
3. Solution **4**
4. Method **4**
4.1 Numerical analysis (WP1) 4
4.2 Coating preparation, characterization, and stability (WP2) 5
4.2.1 Synthesis and coating 5
4.2.2 Characterization 6
4.2.3 Durability and stability analysis 6
4.3 Experimentation and performance assessment (WP3) 7
4.3.1 Ice adhesion 7
4.3.2 Freezing experiments 8
4.3.3 Impacting droplet freezing experiments 8
5. Innovative Aspect **9**
6. Applicability **10**
7. Estimated cost and Project Scheduling **11**
8. Target Group of the Project Idea (Users): **12**
9. Risks **12**
9.1 Numerical analysis: 12
9.2 Material preparation and characterization 12
10. Resources and Report Layout **13**

Project Detail Report

1. Project summary

Wind energy is the fastest-growing source of electricity generation worldwide and it is considered the main source of renewable energy for electricity production (~9% of total electricity demand in Turkey). Icing is the most significant obstacle to the integrity of wind turbines in cold weather. This project proposes a nano-scale coating that eliminates the risk of icing by preventing condensate accumulation, ice nucleation and ice propagation. The coating performances in terms of coating stability as well as delay in ice formation and heat transfer during the impact of droplets were assessed using computational and experimental approaches. According to our preliminary un-optimized results, the icing time was found to be increased up to 400%. The aims of this project are to improve the wind energy production share by 5%, to result in 10% reduction in repair-induced composite materials produced in the wind industry, and to generate a paradigm shift in a broader context by causing a shift from active de-icing methods to passive anti-icing approach for different energy and transport industries. Fig. 1 shows the general overview of the project.

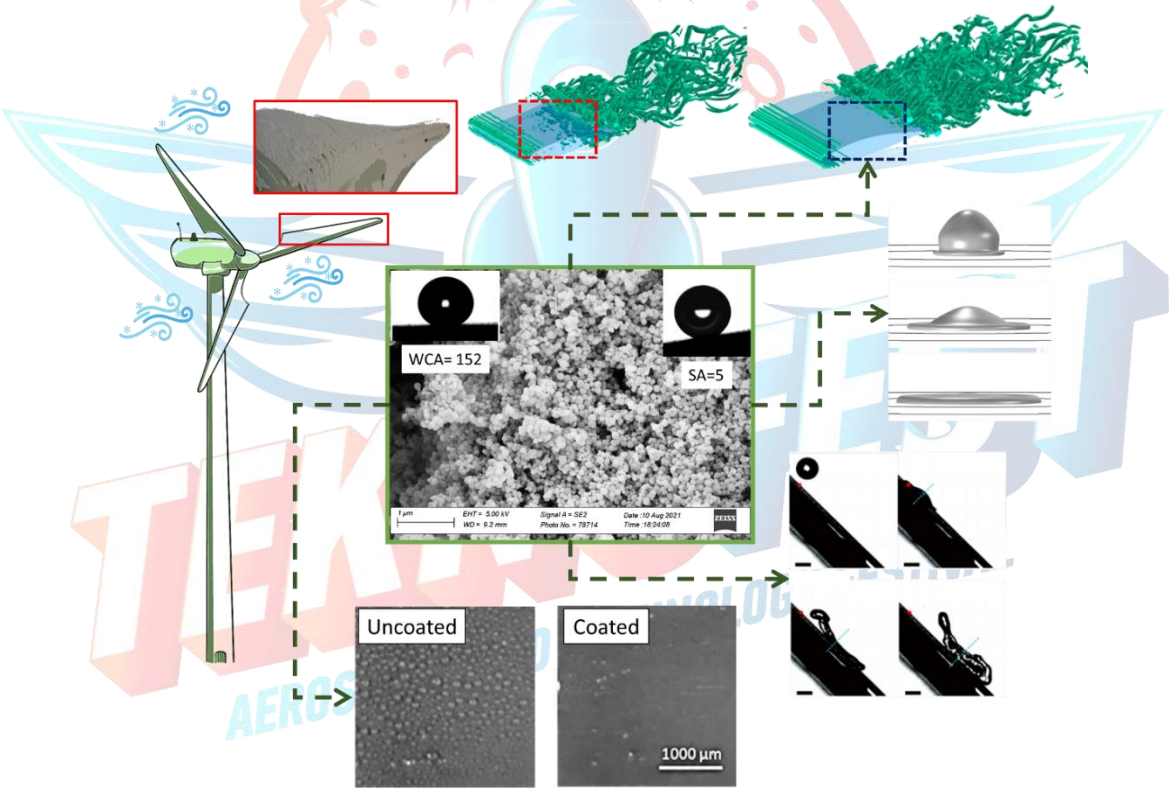

Figure 1. Overall view of the project

2. Problem/ Issue

Wind turbines operate at high altitudes and frequently experience icing on their blades. Icing deteriorates the wind turbine output and reduces the safety in engineering applications. Not only safety in the form of ice detachment from the blades is an important issue, but also the presence of ice during the operation negatively affects the blades and results in an increase in power loss (20-50% power coefficient reduction) and mechanical failure (due to vibration and load increase). Although the control of icing by applying external energy including heating, mechanical, or chemical approaches may be possible, these conventional methods are costly and impractical. On the other hand, passive methods such as coatings and structured surfaces

suffer from a lack of ability to prevent icing conditions. The available passive methods either are superhydrophobic (SHC) blocking condensation and ice accumulation or slippery (LIC) preventing droplet accumulation and ice adhesion. The applicability of the SHCs for real-world applications is questionable mainly due to the loss of functionality at low temperatures (<-15°C). Also, SHCs suffer from inability in suppressing ice nucleation and impede frost formation. Figure above shows the advantages and disadvantages of passive methods (SHCs and LICs).

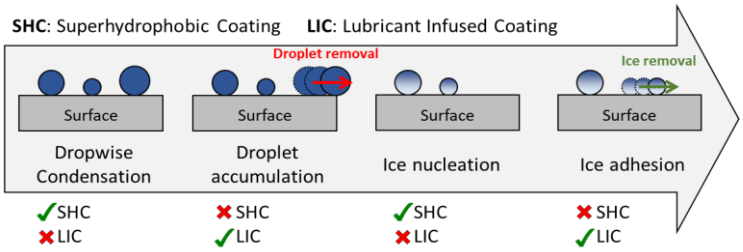

3. Solution

As can be seen in figure to the right, the proposed coating leverages the strengths of SHCs and LICs, this project proposes combined superhydrophobic (anti-icing) and liquid infused (ice-phobic) coatings to eliminate the icing risk and increase the efficiency of wind turbines. The Scanning Electron Microscope (SEM) images of the samples are shown in section 4.2.2. The coating is a superhydrophobic porous structure filled with a lubricant to provide the slippery nature to the coating. Thanks to its unique structure, the proposed coating has both icephobicity and anti-icing properties. While the superhydrophobic feature of the coating remarkably reduces the number of condensed droplets and nucleated ice embryos, its lubricated nature provides favorable conditions for droplet removal and ice shedding. Here, by combining dense nanoscale topography the coating offers promising resistance against condensation-induced wetting and display anti frosting behavior.

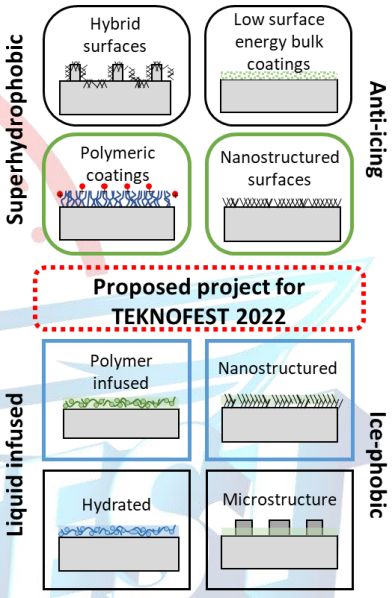

4. Method

This project consisted of three work packages (WPs), one for modeling and numerical analysis (WP1), one for synthesis, characterization, stability, and durability analysis of the coatings (WP2), and one for experimentations and analysis of the obtained results (WP3).

4.1 Numerical analysis (WP1)

WP1 focused on developing a model (COMSOL Multiphysics + MATLAB software) that can analyze dynamics and freezing of impacting droplets and provide droplet dynamics and interfacial heat transfer rates for better analysis of obtained results at WP3. Fig. 2 show the results obtained from the impacting droplets on a surface. The effect of surface wettability on droplet shape during the impact is evident from the Fig. 2a. As can be seen, droplet spreading during the first stage of the impact is more pronounced in hydrophobic surface (90°<WCA<150°) compared to superhydrophobic one (WCA>150°). Fig. 2b shows the complete stage of droplet spread on a superhydrophobic surface. These results were used to analyze the experimental results obtained from high-speed camera. In computational model, the continuum surface force $\kappa=-\nabla.(\nabla\alpha/|\nabla\alpha|)$ is utilized to model the surface tension as an interfacial force in the momentum equation as shown below:

$$\partial\left(\rho\vec{V}\right)/\partial t+\nabla.\left(\rho\vec{V}\vec{V}\right)=-\nabla P+\nabla.\left[\mu\left(\nabla\vec{V}+\nabla\vec{V}^{T}\right)\right]+\gamma\kappa\nabla\alpha+\alpha BV \quad (1)$$

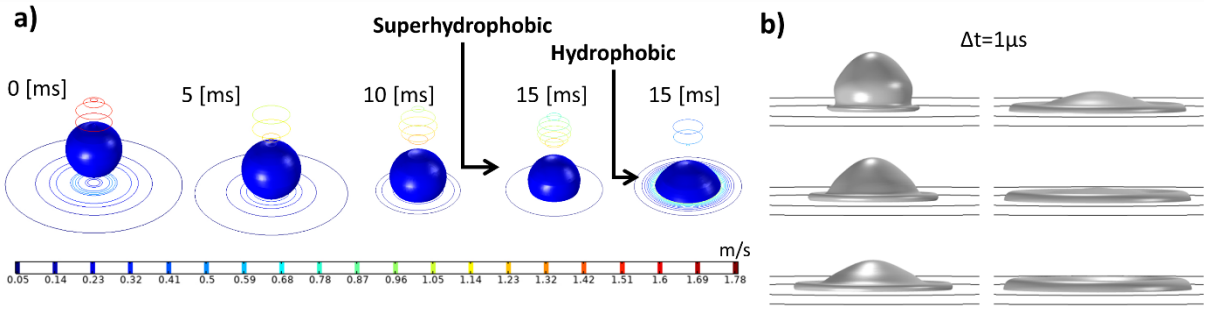

Figure 2. a) Impacting droplet dynamics on hydrophobic and superhydrophobic surfaces (i) hydrophobic (θ=120°) (ii) superhydrophobic (θ=150°); b) Droplet dynamics during the impact for D=100μm and v=50m/s

4.2 Coating preparation, characterization, and stability (WP2)

4.2.1 Synthesis and coating

To achieve superhydrophobic surfaces with lubricity, metal organic frameworks (MOF) is used. Ligand-based method is used to synthesize MOFs. The angle between metal-ligand-metal is about 145 °. This angle is close to Si-O-Si angle in the zeolitic structures, for that reason with ZIFs zeolitic architectures are obtained (Fig. 3a). For ZIF structures imidazolate-based ligands are used and the metal atoms are coordinated through the nitrogen atoms in the ligand. ZIF-8 is a common structure and the ligand used is 2-methylimidazole which contains a methyl group. This methyl group gives its hydrophobic nature. Due to their cage structure, MOFs have a very high specific surface area. By changing the synthesis conditions, the interparticle pore size can be modified, which also affects the specific surface area (Fig. 3). Under normal conditions, the size of the cage cannot be modified. However, high rates of stirring result in hierarchical pores. As a result, higher total pore volumes was achieved. This is very critical for the project proposal since lubricants will be introduced into the coatings through these pores. It is important to mention that superhydrophobic MOFs are used to absorb nonpolar liquids. With a higher total pore size, more liquid can be introduced into the structure. For the ZIF-8 synthesis there are various methods but in this project proposal microwave solvothermal method was used. This method is much faster, and the parameters can be controlled more easily. The synthesis was conducted in an Anton-Paar microwave reactor. 1 mmol of zinc nitrate hexahydrate ($Zn(NO_3)_2.6H_2O$) and 1 mmol 2-methylimidazole was dissolved in 25 mL of N,N-dimethylformamide (DMF). This solution was poured into the glass vials and put into the reactor. The solution was heated to 120 °C and was kept at that temperature for 3 hours. During this synthesis step, the different stirring rates was tested (0-1200 rpm). At the end of the reaction, the solid part was filtered and washed with DMF several times. Then the powder was kept in methanol for 1-2 days then dried at room temperature. Using silanes for coating powder materials as a hydrophobic surface is a common method. To coat ZIF-8, 1H,1H,2H,2H-perfluorooctyltriethoxysilane (POTS) was used. An ethanol suspension of 5% POTS and 1% ZIF-8 was prepared by sonication. The final mixture was applied by an air spray to the surface cleaned with alcohol and acetone. After obtaining the coatings, the surfaces was exposed to Krytox 101. By dipping the materials into liquid, ZIF-8 was allowed to absorb the liquid (Fig. 3b). Since surface tension, viscosity, and vapor pressure are among the parameters that affect

the stability and functionality of the proposed lubricants [1-3], further investigations with different lubricants is planned in near future for TRL>6 applications. In addition to lubricant type, the effect of different spray rounds (sprayed layers) will also investigated by spraying 1, 2, and 3 layers of final mixture to the substrate, to increase its durability (refer to task 4.2.3). For 2 and 3 layered coatings, the lubricants will also contain POTS component in the 1st and 2nd layers.

4.2.2 Characterization

This task focuses on the characterization of prepared coating using different characterization methods including specific surface measurement, X-ray Diffraction Characterization, Scanning Electron Microscopy (SEM), Infrared Fourier Transform Spectroscopy, and Contact angle measurements. For the specific surface area measurements, the BET device is used. After the drying step, the surface area of ZIF-8 powders is measured. One of the main reasons for synthesizing framework structures is to obtain high surface areas. Additionally, N_2 desorption is characterized to provide information on the pore size distribution of the material. With XRD technique, detailed crystallographic information is obtained. For all dried ZIF-8 powders, this characterization will be performed. Using SEM technique, high magnification of the materials can be obtained. This allows observing the morphology at the nanoscale. The coating should be covering all the surfaces with homogenous distribution of the MOF nanoparticles. In addition to SEM, EDX analyses is performed to observe elemental distribution on the surface. Using the FTIR characterizations, the bonds between the metal atom and ligands will be confirmed. Water contact angle (WCA) measurements is performed to characterize the static and dynamic contact angles on coated samples. The SEM image and WCA values are provided in Fig. 3a.

4.2.3 Durability and stability analysis

This task is designated to investigate the stability and durability of the coatings in terms of lubricant dynamics, variations in wetting properties, and functionality at operating conditions. Here, the effects of different parameters such as ambient content (temperature and relative humidity), and testing conditions droplet impact size/velocity, temperature and humidity) on the lubricant depletion (evaporation, cloaking, flowing, wetting ridge), erosion, abrasion, and surface wettability will be investigated. Droplets will be placed on the substrate and visualized using high speed camera to observe the ***lubricant dynamics*** and evaporation for stationary or sliding droplet at different substrate temperatures ranging from 20 to 60°C (on a controlled temperature hotplate) (Fig.3b). The obtained results will be used to study the liquid-liquid (droplet - lubricant), liquid-gas (lubricant/droplet - air/vapor) and liquid-solid (lubricant/droplet - coating) interfaces. The wetting ridge height will be evaluated using visual results, and ridge volume can be calculated by $V_{loss}(L) = \int 2(a+wr_{ext})\Delta h dL + V_0$, where, L is droplet movement distance, $a+wr_{ext}$ is total radius of droplet, w a geometric factor to account for the added width of the wetting ridge, and V_0 is the volume of the wetting ridge of size $r_{ext,0}$ created when the droplet is first placed on the surface, Δh is the difference between front and behind films heights of moving droplet (Fig.3c) [4]. For ***surface wettability*** (WCA, SA, CAH), the contact angle measurement device will be used to characterize the alteration in wetting properties of the coating before and after icing/de-icing cycles and freezing tests. The rainfall ***erosion*** will be simulated by using spray (0.5-1mm with 20-30m/s) [5]. At the end of this task, synthesized coatings will be evaluated according to i) wetting ridge height, ii) wetting ridge volume, iii) decrement in coating wettability (WCA, SA, CAH), v) lubricant evaporation time. The obtained

microscopic images on the satellite droplets on LIC and a very low wetting ridge on the proposed coating is evident from Fig. 3d. Based on obtained results recommendations for the **applicability and possible real problems that may run into at full scale will be made for future TRL6≤ studies.**

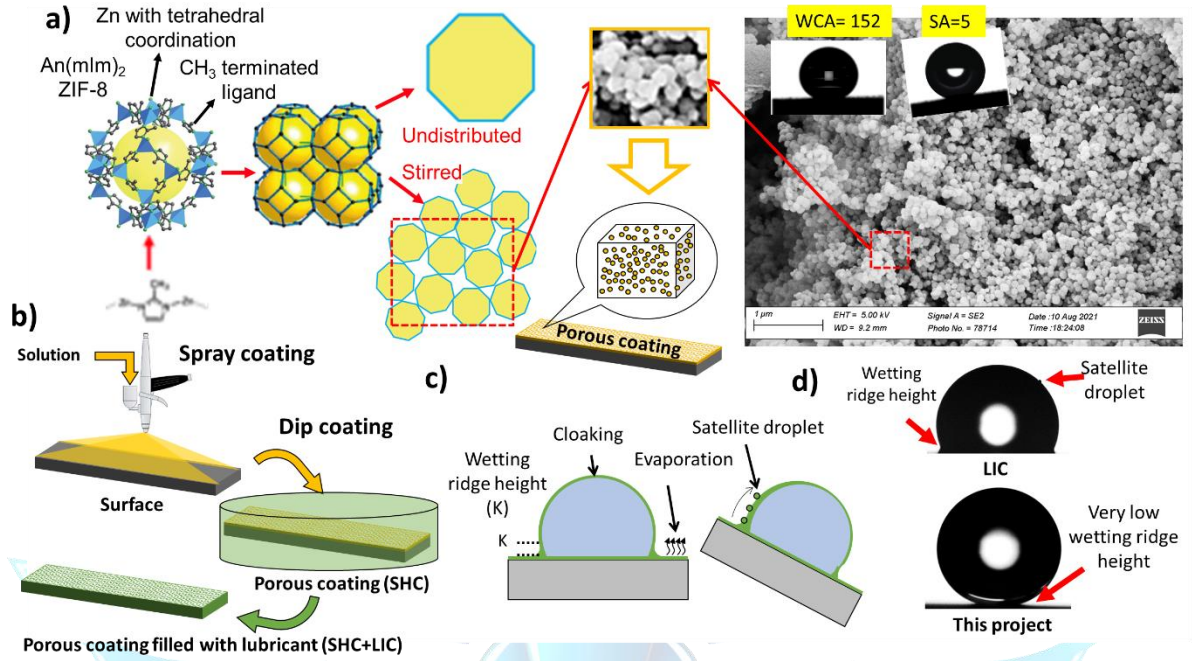

Figure 3. a) ZIF-8 structure, the effect of stirring, the preliminary studies; b) Schematic of coating preparation steps, c) Schematic of wetting ridge, cloaking and evaporation for stability analysis, d) The absence of satellite droplets on proposed coating in this project. Compared to LIC very low wetting ridge was observed in the proposed coating

4.3 Experimentation and performance assessment (WP3)

The **Experimental Conditions** (***Exp.Cond.***) are Droplet sizes of 20,50,100,400µm, impact velocities of 0,5,50 m/s, impact angles of 5,45,90°; temperatures of -40,-20,-10,-5°C; Ambient relative humidity (RH) of 20,50,100%

4.3.1 Ice adhesion

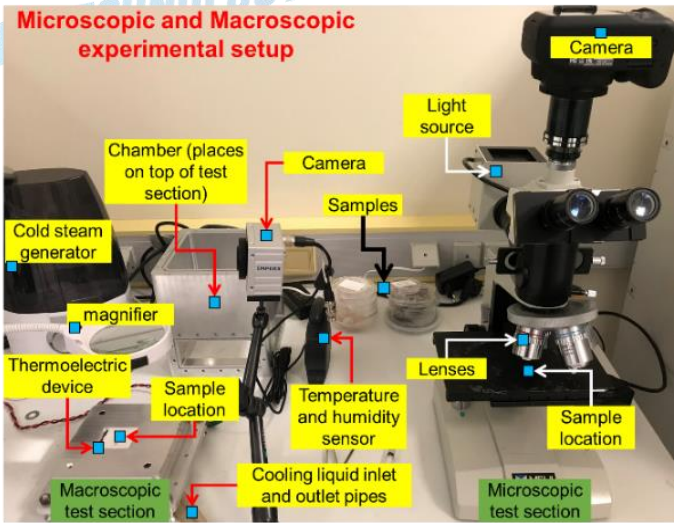

The intensity of ice adhesion is a parameter that can be used to determine the level of ice-phobic or anti-icing nature of a coating. For this, a cylindrical polypropylene chamber (diameters ranging from 0.3 to 1 mm and length 1-3.0 mm) is located on the sample surface, and then filled with water and cooled down to be frozen. Next, the sample is fixed to the cold chamber. Experiments will be performed for shear force analysis on different coatings and temperatures (-40≤T<0°C). The mass, cross-section shape, area, and height of ice are selected based on the standards [6]. Van der Waals, electrostatic, hydrogen bonding, and mechanical adhesion

interactions are acting forces at the ice/coating interface. Compared to van der Waals force, a low electrostatic force has a stronger effect mainly due to rapid reduction in former with distance than latter. The electrostatic forces change with the material's dielectric constant (ε_r), where ice adhesion has been reported to deteriorate with ε_r value. Polar molecules of ice with an exposed hydrogen atom make a strong bond with the surface due to hydrogen bonding. Furthermore, on the microscopic level, the interlocking of microscopic rough elements also induces mechanical adhesion at the ice/interface [7]. The ice adhesion at different surface temperatures, ice/deicing cycles, and coatings properties will be analyzed in this task.

4.3.2 Freezing experiments

The freezing experiments were performed to characterize the icing on coated and uncoated samples. For this, samples are located in a chamber, in which the surface temperature are reduced to specified temperature in *Exp.Cond.*. The chamber humidity was regulated using cold steam and N_2 gas. Two cameras were used to characterize the droplet icing (from side) and icing propagation speed and ice coverage (top). Fig. 4a shows the obtained results for experiments at RH=100% and surface temperature of -20°C. The coated surface remarkably reduced the icing propagation speed and ice coverage ratio. To further investigate the icing, tests were performed for impacting droplets on supercooled surfaces (section 4.3.3)

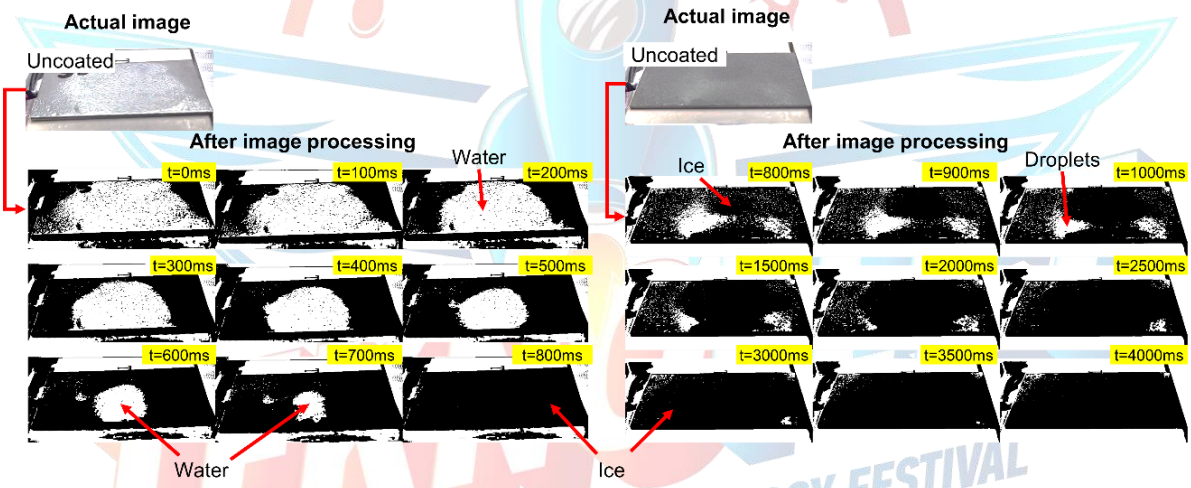

Figure 4. Ice propagation and coverage speed on coated and uncoated samples. The black and bright regions after image processing indicates ice and water, respectively

4.3.3 Impacting droplet freezing experiments

The thermal resistance network of the droplet (stationary or impacting, horizontal or inclined) on the surface is shown in Fig. 5a. The transient heat transfer from surface to the droplet can be used to measure the required time for droplet icing at different conditions. Furthermore, the droplet experiences three phases of spreading, retraction, and rebounding upon impact [8] (Fig. 5b). Maximum droplet spread, shrink rate, and spreading time are the main parameters for spreading and retraction stages. The maximum droplet spreading, which is an indication for maximum coating/droplet contact area, is a significant parameter in heat transfer from droplet to the coated surface. While non-dimensional maximum spread factor ($\beta_{max}=D_{max}/D_0$) can be used to characterize the impact dynamics, shrink rate ($\beta_{real}=D_{final}/D_{max}$) can be used to quantify the freezing aspect during the shrinking stage [9]. The required time for an impacting droplet to reach the maximum spreading is referred to as spreading time (t_{max}). High-speed imaging analysis assists us to characterize the spreading time as well as shrinking time. The latent heat

of supercooled ($Q_c = (c\Delta T + q_l)\rho\frac{\pi D_0^3}{6}$), the heat transfer rate at the droplet/surface interface ($Q_f = hS\Delta T = \frac{Nuk\Delta T}{l}.\frac{\pi(\beta 0^2{}_{max}}{4\,Re^{0.8}\,D_0\frac{0.166\,Pr^{0.6}\,k\pi\beta^2_{max}}{Y_c}}$), and freezing time are three parameters that are used to quantify the transient heat transfer rate during the droplet impact [10]. Fig. 5c shows the compared results for the different surfaces in the literature [11]. As can be seen, superhydrophobic surfaces have lower freezing time (t_{freeze}), while lubricated surfaces provide larger maximum diameter. The proposed coating has lower maximum diameter and higher freezing time. The evolutions of droplet contact time (Fig. 5d), freezing onset time, and rebounding mass fraction at different conditions will be investigated on impacting droplets on inclined surfaces. The slippery effect will be considered by decomposing the normal and tangential velocities (V_n and V_t, respectively). By considering the tangential Reynolds number, the heat transfer rate due to the slipping effect is estimated by $Q_s = \theta_0\tau_{final}h_D = \theta_0\tau_{freezing}\frac{0.664\,Re_h^{0.5}\,Pr^{1/3}\,k}{D_{final}}$. Here, h_D is convective heat transfer (calculated from Nusselt number and compared with numerical results), and D_{final} and $\tau_{freezing}$ will be obtained experimentally. Here, additional parameter of H' (H'=H/D_0) will be defined to characterize the maximum height of the primary and secondary (splashed) droplet perpendicular to the surface during the retracting stage [12]. The dynamic of the droplet will be characterized using droplet Weber ($We=\rho D_0V^2/\sigma$) number, impact diameter, velocity, and angle. The fractions, dimensions, and velocity of splashed droplets will be obtained for estimation of secondary impact effect (can be estimated by the primary impacts with similar size, angle and velocity) [13].

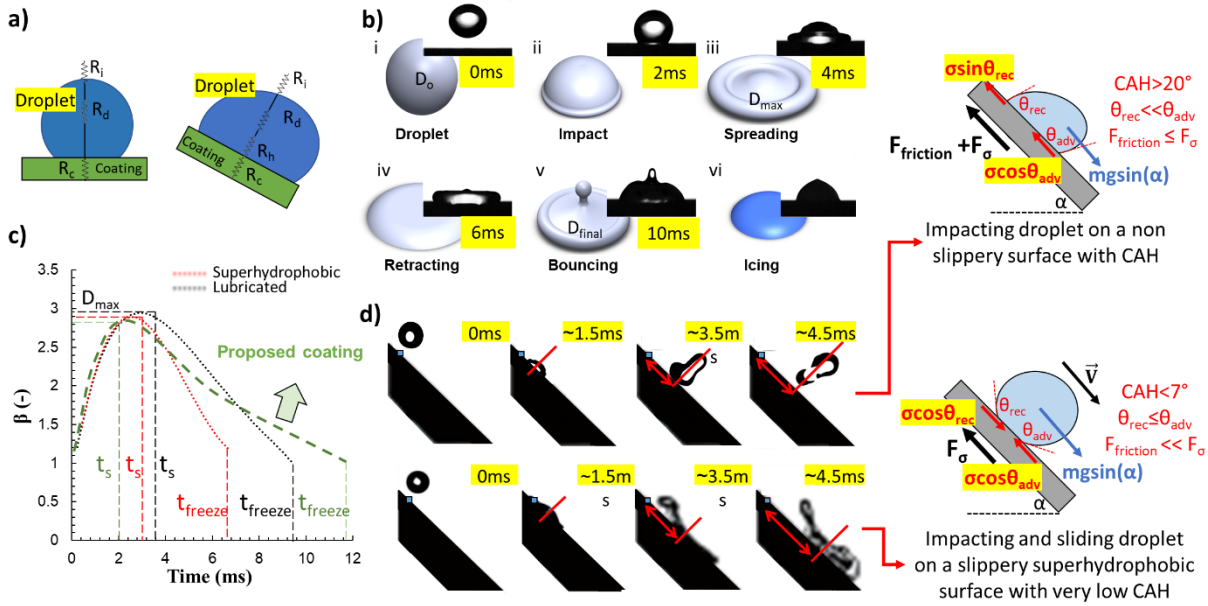

Figure 5 a) Thermal resistance model for droplets; b) Results on stages of impacting droplet and freezing; c) Maximum spread factor and freezing time; d) Impact dynamics on inclined superhydrophobic surface

5. Innovative Aspect

The information on the preparation and characteristics if the coating is provided in previous section. From commercial point of view to the best of our knowledge, there is no available commercialized coating to eliminate the icing on surface of any kind in the relevant industry. In terms of state-of-the-art, there are several studies in the literature proposing SHCs or LICs.

There are only two study proposing slippery surfaces with superhydrophobic properties. But since surface roughness introduces boundary layer transition complexity and increases the drag coefficient in airfoils, the adaptation of a coating with microstructure patterns may not be applicable for the wind industry. Therefore, the nano-scale coating proposed in this project will be the first of its kind. Furthermore, SHCs are mechanically weak against external forces and icing shear removal cycles and stop functioning when exposed to low temperature and high vapor contents. Furthermore, on micro-structured slippery coatings, the lubricant can be lost easily from the valley of the microscale features and can lead to exposure of the top of the underlying substrates, and this may block the mobility of the droplets. By addressing the shortcomings of the available techniques, the proposed nanoscale coating substantially reduces the risk of icing at saturated and supersaturated conditions. A summary of the available recent studies is shown below. Here, "μ", "n" and "μn" prefixes stand for microscale, nanoscale, and combined micro and nanoscale coatings, respectively. IAS is Ice Adhesion Strength, WCA is Water Contact Angle, CAH is Contact Angle Hysteresis, and SA is Sliding angle.

Reference	Type	IAS (kPa)	WCA	CAH	SA	Reference	Type	IAS (kPa)	WCA	CAH	SA
[14]	μ-SHC	NA	156	NA	NA	[15]	n-SHC	NA	161	NA	NA
[16]	n-SHC	NA	168	3	NA	[17]	n-SHC	NA	165	NA	1
[18]	μn-SHC	NA	151	NA	NA	[19]	μn-SHC	NA	150	NA	8
[20]	μn-SHC	16.3	154	12	NA	[21]	μn-SHC	51	154	3	NA
[22]	μn-SHC	53.6	155	NA	5	[23]	μn-SHC	NA	156	NA	NA
[24]	μn-SHC	2.65	161	NA	2	[25]	μn-SHC	NA	160	0	NA
[26]	μn-SHC	NA	164	NA	4	[27]	μn-SHC	NA	161	NA	1.4
[28]	μn-SHC	64	170	NA	3	[29]	μ-SHC	50	168	NA	5
[30]	μn-SHC	NA	172	NA	3	[31]	μn-SHC	NA	180	NA	NA
[32]	n-LIC	7	84	34	NA	[33]	n-LIC	17	NA	5	NA
[34]	n-LIC	NA	103	NA	11	[35]	n-LIC	NA	132	NA	29
[36]	n-LIC	NA	90	NA	10	[37]	n-LIC	NA	111	NA	10
[38]	n-LIC	6.2	105	NA	5	[39]	n-LIC	NA	120	NA	8.5
[40]	n-LIC	NA	100	NA	4	[41]	n-LIC	NA	120	5	NA
[42]	n-LIC	NA	109	2	NA	[43]	n-LIC	NA	104	<3	NA
[44]	μn-LIC	4	104	NA	NA	[45]	μn-LIC	6	98°	NA	NA
[46]	μn-LIC	NA	104	NA	NA	[47]	μn-LIC	<1	108	10	NA
[48]	μn-LIC	NA	162	NA	9	[49]	μn-LIC	5.0	109	6	NA
[47]	μn-LIC	0.65	108	5.5	NA	[43]	μn-LIC	6.2	106°	NA	5
[50]	μn-LIC	NA	120	5	NA	[51]	μn-LIC	25	92	NA	5
[52]	μn-LIC-	12	115	NA	3	[53]	μn-LIC	NA	NA	2.5	5
[54]	μn-LIC	NA	107	1.4	NA	[55]	μn-LIC	8	112	1	1
[56]	μ-LIC-SHC	NA	180	25	60	[57]	μ-LIC-SHC	38	150	NA	10
This study	n-LIC-SHC	< 10	>150	<7	<7						

6. Applicability

The proposed technique not only addresses the limitations of available passive methods, but it is durable, has low cost, has lower complexity, and most importantly, it is adaptable for large scales via cold spray coating method. The proposed coating not only is suitable for metallic surfaces, but our preliminary results also indicated the applicability of the coating for composite materials (materials being used in wind industry). Figures above shows the actual blades that are manufactured by the TPI Company. The implementation of the coating to the turbine blades will be performed using spray coating. Since spray coating is currently used by the wind turbine manufacturers to coat the blades with anti-corrosion paint, addition of a second round of spray (anti-icing coating) will be easy to be implemented on site. After that, the coating will be waited for 1-2 day(s) at room temperature to dry, and the coated part will be ready for use. The

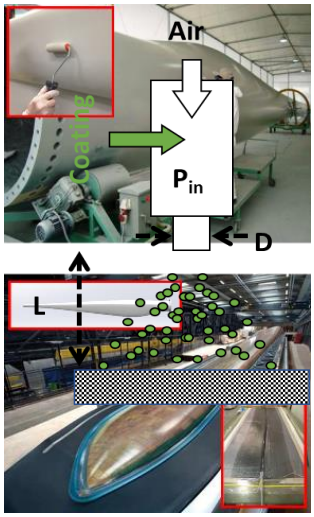

manufacturers have already use spray coating and there is no risk of coating process. Saying that, as shown in figure to the right, utilization of the coating in actual working environment requires additional optimization (inlet pressure - P_{in}, nozzle size - D, distance - L) and inspection (uniformity), which is the matter of higher TRL levels than the proposed lab-scale study (max TRL5). Although the feasibility analysis is mainly applicable for >TRL5 studies, in terms of cost analysis, more than 13% of the annually manufactured blades require icing-induced repairing, with total repair cost of 4.5M€. Approximately the cost of painting of blades is 4M€. It is estimated that the anti-icing coating increases the paint cost by a maximum of 15%, that is, a maximum of 5.75€/Lit (**0.6M€/yr paint price increment vs. 4.5M€/yr repair cost)**. The proposed project also addresses the objectives of Eleventh Development Plan (On Birinci Kalkınma Planı) and it aims to enhance the wind energy capacity by 5%, which is in line with the targeted 38,8% share of renewable resources in electricity generation by 2023. The research group has already file a patent application for the proposed coating as passive anti-icing method for different applications such as renewable energies (solar and wind), aviation (motor air intake and sensing devices), self-cleaning (water-free paths), and transmission lines.

7. Estimated cost and Project Scheduling

All the necessary equipment for testing and characterization are located in Sabanci University. The project's technology readiness level is at TRL4. Additional and more comprehensive tests will be performed on the coating at different droplet, surface and ambient conditions (i.e., velocity, angle, temperature, humidity, etc.) to increase the readiness level to TRL5 or 6. The required materials (consumables) for TRL scale up are provided in Fig. 6a. The main expenses are at the Q2 and Q3 of project. In the last quarter the costs are only for purchasing the actual wind turbine blade composite material for testing. It should be noted that there are no available coating in the relevant industry for cost comparison. Also, the project calendar along the costs are provided in Fig. 6b.

a)

Consumable	Price	Consumable	Price
2-Methylimidazole / 25 g	1,756 TL	Krytox 101 and 103	9,680 TL
N,N-Dimethylformamide anhydrous, 99.8% / 2 L	5,823 TL	1H,1H,2H,2H-Perfluorooctyltriethoxysilane / 25 g	7,660.5 TL
Zinc nitrate hexahydrate / 100 g	1,586 TL	Methanol anhydrous, 99.8% / 2 L	1,954 TL
		Composite blades	10,000 TL
		Total Cost	38,459 TL

b)

WP	Month											
	Q1			Q2			Q3			Q4		
	Mar-22	Apr-22	May-22	June-22	July-22	Aug-22	Sep-22	Oct-22	Nov-22	Dec-22	Jan-23	Feb-23
1												
2.1												
2.2												
2.3												
3.1												
3.2												
3.3												

Expenses	7,470 TL	9,606 TL	11,383 TL	10,000 TL

Figure 6. a) Project's required consumable budget, b) project plant and quarterly budgets

8. Target Group of the Project Idea (Users):

At this stage, the target group of the project is wind turbine blade manufacturers. The research group has already discussed the idea with TPI Composites. In the second stage, the main target of the technology is renewable energy industry such as solar panel and wind turbines and with the help of Sabanci University Industry Relationship office, we will search the possible users in this field (such as LM Wind Power, SolarAPEX). We will also exploiting the technology's applications in other areas such as aviation. The developed technology can also be integrated in civil engineering applications such as bridge cables.

9. Risks

9.1 Numerical analysis:

Risks: Despite the strong background of the group in numerical analysis and simulation, the following problems in convergence may be encountered during the modeling. **R1)** Convergence problem for high droplet impact velocities due to air compressibility and droplet deformation between droplet and surface before impact.

Plan Bs: The following approaches can be used to eliminate the convergence: **B1i)** Utilization of different convergence approaches such as fully coupled, segregated methods, and sequential solution such as in the fluid flow. **B1ii)** Using orders of magnitude smaller time scales (down to 1×10^{-23}) can solve the divergence issue. **B1iii)** The model can be changed to a quasi-steady model and be linked at different time scales.

9.2 Material preparation and characterization

Risks: **R2)** Obtaining ZIF-8 particles with low specific surface areas and pore volumes. **R3)** Obtaining ZIF-8 particle size that is suitable for hydrophobic property. **R4)** The coating may not be homogenous and not we adhesive. **R5)** Obtaining contact angles may be below 150°

Plan Bs: **B2)** In this case, ZIF-8 can be synthesized with other methods. One of these methods is solvothermal with conventional heating setup. In this setup, under similar conditions the ZIF-8 can be synthesized in an oven. Another technique is dry heating; in this technique dry precursors are mixed and put into an autoclave and heated to 120 °C for 24 hours then washed [58]. **B3)** For obtaining different particle sizes, the methods in described in B2.1 can be used. Every synthesis method will result in different particle size range [58]. **B4)** The first thing that can be applied for this situation is using a dip coating setup with a slow raising rate. The coating mixture may not be wetting the surface. For that situation the surface can be treated with plasma or ozone before coating. The silane component may need better interacting functional groups. Before coating, the surface can be coated with a SiO_2 sol-gel. Another coating can be an epoxy-based polymer. The surface can be coated with an epoxy resin then cured. **B5)** If the hydrophobic properties are not enough, ligands with better polarities can be used. TheZIF-8 is not the only MOF that can be used. The novelty of the project does not come from ZIF-8. Instead of 2-methykimidazole, 4-5 dicholoroimidazolate can be used with methanol at room temperature to synthesize ZIF-71 [59]. The probability and impact of the major risks are provided in the figure to the right.

Major risks	Probability (0-10)	Impact (0-10)	Plan B
R1	7	5	B1
R2	6	3	B2
R3	2	9	B3
R4	4	8	B4
R5	3	8	B5

10. Resources and Report Layout

1. Peppou-Chapman, S., J.K. Hong, A. Waterhouse, and C. Neto, *Life and death of liquid-infused surfaces: a review on the choice, analysis and fate of the infused liquid layer.* Chemical Society Reviews, 2020. **49**(11): p. 3688-3715.https://doi.org/10.1039/D0CS00036A
2. Chen, X., G. Wen, and Z. Guo, *What are the design principles, from the choice of lubricants and structures to the preparation method, for a stable slippery lubricant-infused porous surface?* Materials Horizons, 2020. **7**(7): p. 1697-1726.https://doi.org/10.1039/D0MH00088D
3. Olad, A., F. Maryami, A. Mirmohseni, and A.A. Shayegani-Akmal, *Potential of slippery liquid infused porous surface coatings as flashover inhibitors on porcelain insulators in icing, contaminated, and harsh environments.* Progress in Organic Coatings, 2021. **151**: p. 106082.https://doi.org/10.1016/j.porgcoat.2020.106082
4. Kreder, M.J., D. Daniel, A. Tetreault, Z. Cao, B. Lemaire, J.V.I. Timonen, and J. Aizenberg, *Film Dynamics and Lubricant Depletion by Droplets Moving on Lubricated Surfaces.* Physical Review X, 2018. **8**(3): p. 031053.https://link.aps.org/doi/10.1103/PhysRevX.8.031053
5. Zhang, Z., L. Ma, Y. Liu, J. Ren, and H. Hu, *An experimental study of rain erosion effects on a hydro-/ice-phobic coating pertinent to Unmanned-Arial-System (UAS) inflight icing mitigation.* Cold Regions Science and Technology, 2021. **181**: p. 103196.https://doi.org/10.1016/j.coldregions.2020.103196
6. Mittal, K. and C.-H. Choi, *Ice Adhesion: Mechanism, Measurement, and Mitigation*. 2020: John Wiley & Sons.
7. Huang, X., N. Tepylo, V. Pommier-Budinger, M. Budinger, E. Bonaccurso, P. Villedieu, and L. Bennani, *A survey of icephobic coatings and their potential use in a hybrid coating/active ice protection system for aerospace applications.* Progress in Aerospace Sciences, 2019. **105**: p. 74-97.https://doi.org/10.1016/j.paerosci.2019.01.002
8. Tembely, M., R. Attarzadeh, and A. Dolatabadi, *On the numerical modeling of supercooled micro-droplet impact and freezing on superhydrophobic surfaces.* International Journal of Heat and Mass Transfer, 2018. **127**: p. 193-202.https://doi.org/10.1016/j.ijheatmasstransfer.2018.06.104
9. Jin, Z., H. Zhang, and Z. Yang, *Experimental investigation of the impact and freezing processes of a water droplet on an ice surface.* International Journal of Heat and Mass Transfer, 2017. **109**: p. 716-724.https://doi.org/10.1016/j.ijheatmasstransfer.2017.02.055
10. Bergman, T.L., A.S. Lavine, F.P. Incropera, and D.P. DeWitt, *Incropera's principles of heat and mass transfer*. 2017: Wiley Global Education.
11. Liu, Y., X. Yan, and Z. Wang, *Droplet dynamics on slippery surfaces: Small droplet, big impact.* Biosurface and Biotribology, 2019. **5**(2): p. 35-45.https://doi.org/10.1049/bsbt.2019.0004
12. Ding, B., H. Wang, X. Zhu, R. Chen, and Q. Liao, *Water droplet impact on superhydrophobic surfaces with various inclinations and supercooling degrees.* International Journal of Heat and Mass Transfer, 2019. **138**: p. 844-851.https://doi.org/10.1016/j.ijheatmasstransfer.2019.04.106
13. Zhang, R., P. Hao, and F. He, *Drop Impact on Oblique Superhydrophobic Surfaces with Two-Tier Roughness.* Langmuir, 2017. **33**(14): p. 3556-

3567.https://doi.org/10.1021/acs.langmuir.7b00569
14. Sun, J., W. Cheng, J.-L. Song, Y. Lu, Y.-K. Sun, L. Huang, X. Liu, Z.-J. Jin, C.J. Carmalt, and I.P. Parkin, *Fabrication of Superhydrophobic Micro Post Array on Aluminum Substrates Using Mask Electrochemical Machining.* Chinese Journal of Mechanical Engineering, 2018. **31**(1): p. 72.https://doi.org/10.1186/s10033-018-0270-1
15. Lu, Y., S. Sathasivam, J. Song, C.R. Crick, C.J. Carmalt, and I.P. Parkin, *Robust self-cleaning surfaces that function when exposed to either air or oil.* Science, 2015. **347**(6226): p. 1132-1135.https://doi.org/10.1126/science.aaa0946
16. Janowicz, N.J., H. Li, F.L. Heale, I.P. Parkin, I. Papakonstantinou, M.K. Tiwari, and C.J. Carmalt, *Fluorine-Free Transparent Superhydrophobic Nanocomposite Coatings from Mesoporous Silica*. Langmuir, 2020. **36**(45): p. 13426-13438.https://doi.org/10.1021/acs.langmuir.0c01767
17. Tombesi, A., S. Li, S. Sathasivam, K. Page, F.L. Heale, C. Pettinari, C.J. Carmalt, and I.P. Parkin, *Aerosol-assisted chemical vapour deposition of transparent superhydrophobic film by using mixed functional alkoxysilanes.* Scientific Reports, 2019. **9**(1): p. 7549.https://doi.org/10.1038/s41598-019-43386-1
18. Heale, F.L., M. Einhorn, K. Page, I.P. Parkin, and C.J. Carmalt, *Dual-scale TiO2 and SiO2 particles in combination with a fluoroalkylsilane and polydimethylsiloxane superhydrophobic/superoleophilic coating for efficient solvent–water separation.* RSC Advances, 2019. **9**(35): p. 20332-20340.http://dx.doi.org/10.1039/C9RA02700A
19. Wang, X., Y. Lu, Q. Zhang, K. Wang, C.J. Carmalt, I.P. Parkin, Z. Zhang, and X. Zhang, *Durable fire retardant, superhydrophobic, abrasive resistant and air/UV stable coatings.* Journal of Colloid and Interface Science, 2021. **582**: p. 301-311.https://doi.org/10.1016/j.jcis.2020.07.084
20. Janjua, Z.A., B. Turnbull, K.-L. Choy, C. Pandis, J. Liu, X. Hou, and K.-S. Choi, *Performance and durability tests of smart icephobic coatings to reduce ice adhesion.* Applied Surface Science, 2017. **407**: p. 555-564.https://doi.org/10.1016/j.apsusc.2017.02.206
21. Brassard, J.-D., J.-L. Laforte, C. Blackburn, J. Perron, and D.K. Sarkar, *Silicone based superhydrophobic coating efficient to reduce ice adhesion and accumulation on aluminum under offshore arctic conditions.* Ocean Engineering, 2017. **144**: p. 135-141.https://doi.org/10.1016/j.oceaneng.2017.08.022
22. Tong, W., D. Xiong, N. Wang, Z. Wu, and H. Zhou, *Mechanically robust superhydrophobic coating for aeronautical composite against ice accretion and ice adhesion.* Composites Part B: Engineering, 2019. **176**: p. 107267.https://doi.org/10.1016/j.compositesb.2019.107267
23. Li, K., X. Zeng, H. Li, and X. Lai, *A study on the fabrication of superhydrophobic iron surfaces by chemical etching and galvanic replacement methods and their anti-icing properties.* Applied Surface Science, 2015. **346**: p. 458-463.https://doi.org/10.1016/j.apsusc.2015.03.130
24. Jiang, G., L. Chen, S. Zhang, and H. Huang, *Superhydrophobic SiC/CNTs Coatings with Photothermal Deicing and Passive Anti-Icing Properties.* ACS Applied Materials & Interfaces, 2018. **10**(42): p. 36505-36511.https://doi.org/10.1021/acsami.8b11201
25. Chen, C., S. Chen, L. Chen, Y. Yu, D. Weng, A. Mahmood, J. Wang, I.P. Parkin, and C.J. Carmalt, *Underoil Superhydrophilic Metal Felt Fabricated by Modifying Ultrathin Fumed Silica Coatings for the Separation of Water-in-Oil Emulsions.* ACS Applied Materials &

Interfaces, 2020. **12**(24): p. 27663-27671.https://doi.org/10.1021/acsami.0c03801
26. Zhang, X., B. Ding, Y. Bian, D. Jiang, and I.P. Parkin, *Synthesis of superhydrophobic surfaces with Wenzel and Cassie–Baxter state: experimental evidence and theoretical insight.* Nanotechnology, 2018. **29**(48): p. 485601.https://doi.org/10.1088/1361-6528/aae187
27. Wu, B., X. Cui, H. Jiang, N. Wu, C. Peng, Z. Hu, X. Liang, Y. Yan, J. Huang, and D. Li, *A superhydrophobic coating harvesting mechanical robustness, passive anti-icing and active de-icing performances.* Journal of Colloid and Interface Science, 2021. **590**: p. 301-310.https://doi.org/10.1016/j.jcis.2021.01.054
28. Emelyanenko, A.M., L.B. Boinovich, A.A. Bezdomnikov, E.V. Chulkova, and K.A. Emelyanenko, *Reinforced Superhydrophobic Coating on Silicone Rubber for Longstanding Anti-Icing Performance in Severe Conditions.* ACS Applied Materials & Interfaces, 2017. **9**(28): p. 24210-24219.https://doi.org/10.1021/acsami.7b05549
29. Wu, X., V.V. Silberschmidt, Z.-T. Hu, and Z. Chen, *When superhydrophobic coatings are icephobic: Role of surface topology.* Surface and Coatings Technology, 2019. **358**: p. 207-214.https://doi.org/10.1016/j.surfcoat.2018.11.039
30. Zhu, T., Y. Cheng, J. Huang, J. Xiong, M. Ge, J. Mao, Z. Liu, X. Dong, Z. Chen, and Y. Lai, *A transparent superhydrophobic coating with mechanochemical robustness for anti-icing, photocatalysis and self-cleaning.* Chemical Engineering Journal, 2020. **399**: p. 125746.https://doi.org/10.1016/j.cej.2020.125746
31. Song, J., L. Huang, C. Zhao, S. Wu, H. Liu, Y. Lu, X. Deng, C.J. Carmalt, I.P. Parkin, and Y. Sun, *Robust Superhydrophobic Conical Pillars from Syringe Needle Shape to Straight Conical Pillar Shape for Droplet Pancake Bouncing.* ACS Applied Materials & Interfaces, 2019. **11**(48): p. 45345-45353.https://doi.org/10.1021/acsami.9b16509
32. Coady, M.J., M. Wood, G.Q. Wallace, K.E. Nielsen, A.-M. Kietzig, F. Lagugné-Labarthet, and P.J. Ragogna, *Icephobic Behavior of UV-Cured Polymer Networks Incorporated into Slippery Lubricant-Infused Porous Surfaces: Improving SLIPS Durability.* ACS Applied Materials & Interfaces, 2018. **10**(3): p. 2890-2896.https://doi.org/10.1021/acsami.7b14433
33. Yamazaki, T., M. Tenjimbayashi, K. Manabe, T. Moriya, H. Nakamura, T. Nakamura, T. Matsubayashi, Y. Tsuge, and S. Shiratori, *Antifreeze Liquid-Infused Surface with High Transparency, Low Ice Adhesion Strength, and Antifrosting Properties Fabricated through a Spray Layer-by-Layer Method.* Industrial & Engineering Chemistry Research, 2019. **58**(6): p. 2225-2234.https://doi.org/10.1021/acs.iecr.8b05927
34. Mao, X., J. Tan, L. Xie, J. Wang, and H. Zeng, *Novel multifunctional solid slippery surfaces with self-assembled fluorine-free small molecules.* Chemical Engineering Journal, 2021. **404**: p. 127064.https://doi.org/10.1016/j.cej.2020.127064
35. Zhang, M., C. Li, S. Yang, J. Hirte, W. Zhao, Q. Wei, Z. Diao, J.P. Spatz, and C. Zhao, *Ultra-transparent slippery surface.* Smart Materials in Medicine, 2021. **2**: p. 38-45.https://doi.org/10.1016/j.smaim.2020.10.001
36. Manabe, K., S. Nishizawa, K.-H. Kyung, and S. Shiratori, *Optical Phenomena and Antifrosting Property on Biomimetics Slippery Fluid-Infused Antireflective Films via Layer-by-Layer Comparison with Superhydrophobic and Antireflective Films.* ACS Applied Materials & Interfaces, 2014. **6**(16): p. 13985-13993.https://doi.org/10.1021/am503352x
37. Cui, J., H. Zhu, Z. Tu, D. Niu, G. Liu, Y. Bei, and Q. Zhu, *Effect of the texture geometry on the slippery behavior of liquid-infused nanoporous surfaces.* Journal of Materials Science,

2019. **54**(3): p. 2729-2739.https://doi.org/10.1007/s10853-018-2972-2
38. Long, Y., X. Yin, P. Mu, Q. Wang, J. Hu, and J. Li, *Slippery liquid-infused porous surface (SLIPS) with superior liquid repellency, anti-corrosion, anti-icing and intensified durability for protecting substrates.* Chemical Engineering Journal, 2020. **401**: p. 126137.https://doi.org/10.1016/j.cej.2020.126137
39. Ouyang, Y., J. Zhao, R. Qiu, S. Hu, Y. Zhang, and P. Wang, *Bioinspired superhydrophobic and oil-infused surface: Which is the better choice to prevent marine biofouling?* Colloids and Surfaces A: Physicochemical and Engineering Aspects, 2018. **559**: p. 297-304.https://doi.org/10.1016/j.colsurfa.2018.09.060
40. Liu, M., Y. Hou, J. Li, L. Tie, and Z. Guo, *Transparent slippery liquid-infused nanoparticulate coatings.* Chemical Engineering Journal, 2018. **337**: p. 462-470.https://doi.org/10.1016/j.cej.2017.12.118
41. Guo, J., W. Fang, A. Welle, W. Feng, I. Filpponen, O.J. Rojas, and P.A. Levkin, *Superhydrophobic and Slippery Lubricant-Infused Flexible Transparent Nanocellulose Films by Photoinduced Thiol–Ene Functionalization.* ACS Applied Materials & Interfaces, 2016. **8**(49): p. 34115-34122.https://doi.org/10.1021/acsami.6b11741
42. Gulfam, R., D. Orejon, C.-H. Choi, and P. Zhang, *Phase-Change Slippery Liquid-Infused Porous Surfaces with Thermo-Responsive Wetting and Shedding States.* ACS Applied Materials & Interfaces, 2020. **12**(30): p. 34306-34316.https://doi.org/10.1021/acsami.0c06441
43. Zhao, H., C.A. Deshpande, L. Li, X. Yan, M.J. Hoque, G. Kuntumalla, M.C. Rajagopal, H.C. Chang, Y. Meng, S. Sundar, P. Ferreira, C. Shao, S. Salapaka, S. Sinha, and N. Miljkovic, *Extreme Antiscaling Performance of Slippery Omniphobic Covalently Attached Liquids.* ACS Applied Materials & Interfaces, 2020. **12**(10): p. 12054-12067.https://doi.org/10.1021/acsami.9b22145
44. Wang, F., W. Ding, J. He, and Z. Zhang, *Phase transition enabled durable anti-icing surfaces and its DIY design.* Chemical Engineering Journal, 2019. **360**: p. 243-249.https://doi.org/10.1016/j.cej.2018.11.224
45. Yuan, Y., L. Wang, G. Liu, and R. Liao, *Fabrication of Ultralow Ice-Adhesion Slippery Liquid Infused Porous Surfaces on Aluminum Alloy (7075-T651).* Coatings, 2020. **10**(11): p. 1025.https://doi.org/10.3390/coatings10111025
46. Chatterjee, R., D. Beysens, and S. Anand, *Delaying ice and frost formation using phase-switching liquids.* Advanced Materials, 2019. **31**(17): p. 1807812.https://doi.org/10.1002/adma.201807812
47. Tas, M., H. Memon, F. Xu, I. Ahmed, and X. Hou, *Electrospun nanofibre membrane based transparent slippery liquid-infused porous surfaces with icephobic properties.* Colloids and Surfaces A: Physicochemical and Engineering Aspects, 2020. **585**: p. 124177.https://doi.org/10.1016/j.colsurfa.2019.124177
48. Wang, H., K. Wang, H. Lu, I.P. Parkin, and X. Zhang, *Flexible and Strong Robust Superhydrophobic Monoliths with Antibacterial Property.* ACS Applied Polymer Materials, 2020. **2**(11): p. 4856-4863.https://doi.org/10.1021/acsapm.0c00792
49. Cui, W. and T.A. Pakkanen, *Fabrication of transparent icephobic surfaces with self-reparability: Effect of structuring and thickness of the lubricant-elastomer layer.* Applied Surface Science, 2020. **504**: p. 144061.https://doi.org/10.1016/j.apsusc.2019.144061
50. Laney, S.K., M. Michalska, T. Li, F.V. Ramirez, M. Portnoi, J. Oh, I.G. Thayne, I.P.

Parkin, M.K. Tiwari, and I. Papakonstantinou, *Delayed Lubricant Depletion of Slippery Liquid Infused Porous Surfaces Using Precision Nanostructures.* Langmuir, 2021.https://doi.org/10.1021/acs.langmuir.1c01310

51. Heale, F.L., I.P. Parkin, and C.J. Carmalt, *Slippery Liquid Infused Porous TiO2/SnO2 Nanocomposite Thin Films via Aerosol Assisted Chemical Vapor Deposition with Anti-Icing and Fog Retardant Properties.* ACS Applied Materials & Interfaces, 2019. **11**(44): p. 41804-41812.https://doi.org/10.1021/acsami.9b14160

52. Juuti, P., J. Haapanen, C. Stenroos, H. Niemelä-Anttonen, J. Harra, H. Koivuluoto, H. Teisala, J. Lahti, M. Tuominen, J. Kuusipalo, P. Vuoristo, and J.M. Mäkelä, *Achieving a slippery, liquid-infused porous surface with anti-icing properties by direct deposition of flame synthesized aerosol nanoparticles on a thermally fragile substrate.* Applied Physics Letters, 2017. **110**(16): p. 161603.https://aip.scitation.org/doi/abs/10.1063/1.4981905

53. Wong, T.-S., S.H. Kang, S.K.Y. Tang, E.J. Smythe, B.D. Hatton, A. Grinthal, and J. Aizenberg, *Bioinspired self-repairing slippery surfaces with pressure-stable omniphobicity.* Nature, 2011. **477**(7365): p. 443-447.https://doi.org/10.1038/nature10447

54. Patir, A., G.B. Hwang, C. Lourenco, S.P. Nair, C.J. Carmalt, and I.P. Parkin, *Crystal Violet-Impregnated Slippery Surface to Prevent Bacterial Contamination of Surfaces.* ACS Applied Materials & Interfaces, 2021. **13**(4): p. 5478-5485.https://doi.org/10.1021/acsami.0c17915

55. Niemelä-Anttonen, H., H. Koivuluoto, M. Tuominen, H. Teisala, P. Juuti, J. Haapanen, J. Harra, C. Stenroos, J. Lahti, J. Kuusipalo, J.M. Mäkelä, and P. Vuoristo, *Icephobicity of Slippery Liquid Infused Porous Surfaces under Multiple Freeze–Thaw and Ice Accretion–Detachment Cycles.* Advanced Materials Interfaces, 2018. **5**(20): p. 1800828.https://doi.org/10.1002/admi.201800828

56. Rico, V., J. Mora, P. García, A. Agüero, A. Borrás, A.R. González-Elipe, and C. López-Santos, *Robust anti-icing superhydrophobic aluminum alloy surfaces by grafting fluorocarbon molecular chains.* Applied Materials Today, 2020. **21**: p. 100815.https://doi.org/10.1016/j.apmt.2020.100815

57. Chavan, S., H. Cha, D. Orejon, K. Nawaz, N. Singla, Y.F. Yeung, D. Park, D.H. Kang, Y. Chang, and Y. Takata, *Heat transfer through a condensate droplet on hydrophobic and nanostructured superhydrophobic surfaces.* Langmuir, 2016. **32**(31): p. 7774-7787.https://doi.org/10.1021/acs.langmuir.6b01903

58. Lee, Y.-R., M.-S. Jang, H.-Y. Cho, H.-J. Kwon, S. Kim, and W.-S. Ahn, *ZIF-8: A comparison of synthesis methods.* Chemical Engineering Journal, 2015. **271**: p. 276-280.https://doi.org/10.1016/j.cej.2015.02.094

59. He, C.-T., L. Jiang, Z.-M. Ye, R. Krishna, Z.-S. Zhong, P.-Q. Liao, J. Xu, G. Ouyang, J.-P. Zhang, and X.-M. Chen, *Exceptional Hydrophobicity of a Large-Pore Metal–Organic Zeolite.* Journal of the American Chemical Society, 2015. **137**(22): p. 7217-7223.https://doi.org/10.1021/jacs.5b03727